Physics and Imaging in Radiation Oncology 7 (2018) 45–50

Contents lists available at ScienceDirect

Physics and Imaging in Radiation Oncology

journal homepage: www.elsevier.com/locate/phro

Original Research Article

# Cone beam CT based dose calculation in the thorax region

Laura Patricia Kaplan[a,b,*], Ulrik Vindelev Elstrøm[a], Ditte Sloth Møller[a], Lone Hoffmann[a]

[a] Department of Medical Physics, Aarhus University Hospital, Nørrebrogade 44, 8000 Aarhus, Denmark
[b] Institute of Physics and Astronomy, Aarhus University, Ny Munkegade 120, 8000 Aarhus, Denmark

ABSTRACT

*Background and purpose:* The limited image quality in Cone Beam CT (CBCT) stemming primarily from scattered radiation hinders accurate CBCT based dose calculation in radiotherapy. We investigated the use of a stoichiometric calibration for dose calculation on CBCT images of lung cancer patients.

*Materials and methods:* CBCT calibrations were performed with thorax scan protocols, using a phantom with approximately the diameter of an average human thorax and a central cavity simulating the thoracic cavity. Thus scatter conditions resembling those in clinical thorax CBCT scans were simulated. A published stoichiometric parametrization was used. A treatment plan was simulated on CBCT and CT scans of an anthropomorphic phantom, the dose distributions were calculated, and clinically relevant DVH parameters were compared. Twelve lung cancer patients had surveillance CT scans (s-CT) taken twice during their treatment course in addition to daily setup CBCTs. Dose calculations were performed on the s-CTs and the corresponding CBCTs taken on the same day, and DVH parameters were compared.

*Results:* Eighty percent of CBCT DVH parameters found for the phantom were within ± 1% of CT doses, and 98% were within ± 3%. For patients, the median CT/CBCT dose difference was within ± 2%, and 98% of DVH parameters were within ± 4%. Minimum dose to the tumor was underestimated (median 1.9%) on CBCT, while maximum doses to most organs at risk were slightly overestimated.

*Conclusion:* Direct dose calculations on CBCTs of lung cancer patients were feasible within ~4% accuracy using a simple calibration method, which is easily implemented in a clinical setting.

## 1. Introduction

Anatomical changes such as baseline shifts, tumor shrinkage, appearance/disappearance of atelectasis or pleural effusion during the radiotherapy (RT) course of lung cancer patients are frequent and may be detrimental for target coverage [1–5]. Furthermore, overdosage of organs at risk (OARs) due to anatomical changes has been observed for lung cancer patients treated with high dose RT [6]. Adaptive radiotherapy (ART) aims at adjusting the treatment plan to the anatomical changes observed and restoring the planned dose distribution. Daily Cone-beam CT (CBCT) scans taken for patient setup may be used to identify patients who will benefit from ART either from visual inspection [2,5] or directly by dose calculation [7–17].

Direct dose calculation based on CBCT images is challenging due to inherent properties of CBCT image quality, which suffers from uncertainties in Hounsfield Units (HU) due to photon scatter, as well as a number of artefacts. Several approaches aiming at minimizing these factors have been proposed. These range from dose calculations on CT images deformed to the daily anatomy as seen on CBCT [7–9], to HU or electron density override in CBCT images [10,11] and finally direct dose calculation on CBCTs utilizing artefact and scatter corrections [11,14–17] or HU to electron density calibrations performed directly on CBCT [9–13,18]. Deviations between doses calculated on CT and CBCT of 1 to 5% were found depending on the method chosen for CBCT calculation [9–18].

Direct dose calculation on CBCT using a HU to electron density conversion curve may be preferable in a clinical setting as it enables daily dose calculation on the CBCT images with no additional steps as compared to CT dose calculation. Scatter conditions differ depending on the anatomical site of the tumor and individual conversion curves may be required for distinct anatomical regions. These conversion curves can be made using either a calibration phantom [9–10,12,18] or previously obtained patient scans [10,12–13]. The latter requires additional acquisition of patient scans and accurate segmentation, increasing the required workload.

To overcome known limitations of CBCT dose calculation stemming primarily from scattered radiation, careful calibration should be made on CBCT scanners in scatter conditions resembling those seen in lung cancer patients. When using a calibration phantom, stoichiometric calibration mitigates calibration inaccuracies arising from the fact that the atomic composition of phantom tissue substitutes is different from that of the actual tissues they represent. These calibration efforts do not

* Corresponding author at: Department of Medical Physics, Aarhus University Hospital, Nørrebrogade 44, 8000 Aarhus, Denmark.
*E-mail addresses:* laukap@rm.dk (L.P. Kaplan), ulrik.vindelev.elstroem@auh.rm.dk (U.V. Elstrøm), dittmoel@rm.dk (D.S. Møller), lone.hoffmann@aarhus.rm.dk (L. Hoffmann).

https://doi.org/10.1016/j.phro.2018.09.001
Received 9 May 2018; Received in revised form 13 September 2018; Accepted 20 September 2018

correct for artefacts stemming from e.g. motion, however.

The purpose of the current study was to obtain CBCT HU to electron density conversion curves for multiple CBCT scanners using the stoichiometric calibration method on a commercial phantom and to investigate the accuracy of the dose calculation on CBCT images. The dose calculation was validated on CBCT images of both an anthropomorphic phantom and twelve lung cancer patients. Additionally, the difference between using a mean curve for all CBCT scanners and individual curves was determined.

## 2. Materials and methods

### 2.1. Calibration

The CIRS Electron Density Phantom (model 062M, CIRS, Norfolk VA; see Fig. S1, Supplementary details) was used to perform stoichiometric calibrations as described in detail by Elstrøm et al. [18], using a slightly modified version of the method proposed by Schneider et al. [19]. Calibration scans were made with the central part of the phantom removed to simulate a thoracic cavity, and six different tissue substitute inserts, ranging in electron density from adipose tissue to cortical bone, were used, as done in previous studies [19,20]. The calibrations were made on a CT scanner (Philips Brilliance Big Bore) and six CBCT imaging systems, CBCT1 to CBCT6 (Varian Clinac 2300IX with OBI v. 1.6.17 Palo Alto, CA). CBCT scans were taken using low-dose thorax protocols (half-beam, half-fan bow-tie, 110 kV, 400 mAs, anti-scatter grid) and CT scans were taken using a thorax 4DCT protocol (120 kV, 1000 mAs). The slice thickness was 3 mm in both cases. The imaging isocenter was placed in the center of the phantom's central cavity. A mean of the CBCT calibrations was taken to construct the final calibration curve. The stoichiometric CT and the mean CBCT calibration curves, as well as the calibration curves corresponding to the individual CBCTs, are shown in Figs. S2 and S3 (Supplementary material).

### 2.2. Phantom dose calculations

CT and CBCT scans of an anthropomorphic thorax phantom (Alderson Radiation Therapy Phantom, Radiology Support Devices, Inc., Long Beach, CA) were acquired on the same six CBCTs and CT scanner, using the same scan protocols that were used for calibration (Fig. S4, Supplementary material).

Artificial target volumes and OARs were delineated on the CT scan of the phantom. A tumor (clinical target volume, tumor; CTV-T) was delineated centrally in the right lung, consisting solely of lung tissue, and lymph nodes (clinical target volume, lymph nodes; CTV-N) were contoured in the mediastinum. Delineated OARs were the bronchi, spinal cord, right lung, and heart. Delineations were only made to the extent visible on the CBCTs, which are shorter along the cranio-caudal axis than the CT scan. A five-field IMRT plan was simulated and optimized to deliver 66 Gy to the target volumes. The structures and treatment plan were rigidly transferred to the CBCT images, and delivered doses were calculated on all scans. All structure delineation and dose calculation was done in the Eclipse Treatment Planning System (Analytical Anisotropic Algorithm v. 13.7.14, calculation grid size 0.2 cm, Varian Medical Systems). Dose-Volume Histogram data was exported and analyzed using MATLAB version R2017a (The Mathworks Inc, Natick, MA, USA). Mean doses to all structures, the dose covering 98% of the CTVs' volume ($D_{98}$), and the maximum dose given to 2% of a structure's volume ($D_2$) were calculated on both CT and CBCT images, using the stoichiometric calibration curves determined for each imaging device. In addition to the mean dose often quoted for target and many OARs, the selected DVH parameters represent near-minimum and near-maximum doses and are relevant for target coverage and OAR over-dosage. The CBCT dose calculations were repeated using the mean calibration curve described in Section 2.1.

### 2.3. Patient characteristics, imaging and dose calculation

Pre-treatment CBCT scans were evaluated for a group of 50 lung cancer patients treated at Aarhus University Hospital in 2013. Details on the treatment of these patients can be found in Møller et al., [5]. All patients had free-breathing 3D-CBCTs taken at every fraction for setup with match on the primary tumor (GTV-T). Low-dose thorax scan protocols were used and the patients were centered (within ± 3 cm) before image acquisition. In addition to this, surveillance 4DCT scans (s-CT) were taken at fractions 10 and 20. Twelve patients were selected for this study based on the criterion that the anatomy and patient positioning on s-CT and CBCT acquired at fractions 10 and 20, respectively, were as similar as possible.

The median [range] gross tumor volume (GTV-T) on planning CT was 40 $cm^3$ [6;146], two patients had no GTV-T delineated, and out of the twelve patients, only seven had lymph nodes (GTV-N) included in the target delineated. The median [range] tumor motion was 2.2 mm [0.3;6.6] cranio-caudal, 1.6 mm [0.7;2.8] anterior-posterior and 1.1 mm [0.6;3.9] left–right at fraction 10, and 2.2 mm [0.7;5.4] cranio-caudal, 1.8 mm [0.8;2.9] anterior-posterior and 1.5 mm [0.3;3.6] left–right at fraction 20. Target and OARs were delineated on the mid-ventilation phase of the s-CTs at fractions 10 and 20 by experienced radiation oncologists and transferred rigidly to the CBCT of the same day using 3D translational shifts and couch rotation. Rigid registration was chosen due to the anatomical similarity seen in s-CT and CBCT. The registrations were made based on soft tissue matches on the GTV-T (or GTV-N) in order to simulate the treatment procedure. Treatment plans were recalculated on s-CT and the corresponding CBCT, with fixed Monitor Units. All treatment plans were IMRT plans comprising five or six fields. Prescribed doses were 66 Gy/33 fractions once daily (ten patients, NSCLC) and 45 Gy/30 fractions twice daily (two patients, SCLC). CBCTs for which field entrance regions were outside the field-of-view were extended to include these regions by copying the top or bottom slice (whichever applied). The same was done if a structure of interest was close to the upper or lower edge of the CBCT field of view to account for photon scatter in the dose calculation.

The s-CTs were acquired on the same CT scanner as was used for calibration and phantom measurements. The specific imaging device used for CBCT acquisition varied between patients, although all were of the type Varian Clinac OBI. Dose calculation and data analysis was done as described in Section 2.2 for the anthropomorphic phantom. Clinically relevant DVH metrics were extracted from s-CT and the corresponding CBCT and compared. The parameters considered were the mean dose and $D_{98}$ for the target volumes, the maximum dose to a volume of 1 cc ($D_{1cc}$) for bronchi, esophagus and spinal cord. For the heart and lung, the volume receiving a certain fixed dose ($V_{xGy}$) was transferred to the CBCT and the dose to this CBCT volume was recalculated ($D_{VxGy}$). For the heart this volume was $V_{25Gy}$ and for the lungs $V_{20Gy}$. These volumes were considered due to the fact that the heart and lungs were not completely included in the CBCT field of view.

## 3. Results

### 3.1. Phantom dose calculation

Eighty percent of calculated DVH parameters showed at most 1% difference between CT and CBCT (mean calibration curve) and 98% of the points were within ± 3% (see Table 1). The median difference between dose parameters calculated using the calibration curve determined on each CBCT separately and those calculated using the mean calibration was 0.0% (min: −1.1%, max: +0.7%).

### 3.2. Patient dose calculation

In twelve patients, anatomy and positioning on s-CT and CBCT acquired at fraction 10 and fraction 20, respectively, were very similar,

**Table 1**
Differences in DVH parameters determined on CBCT and CT images of the Alderson Radiation Therapy Phantom. CBCT doses were calculated using the mean calibration curve. Values are shown as percentage of the CT dose. Positive values indicate that the CBCT dose is higher. Differences above 1.0% are shown in italics.

| | CTV-T | | | CTV-N | | | Bronchi | | Spinal cord | | Heart | | Right lung | |
|---|---|---|---|---|---|---|---|---|---|---|---|---|---|---|
| | $D_{98}$ | $D_{mean}$ | $D_2$ | $D_{98}$ | $D_{mean}$ | $D_2$ | $D_{mean}$ | $D_2$ | $D_{mean}$ | $D_2$ | $D_{mean}$ | $D_2$ | $D_{mean}$ | $D_2$ |
| | *Percentage of CT dose* | | | | | | | | | | | | | |
| CBCT 1 | −1.0 | −0.7 | −0.8 | 0.2 | 0.3 | −0.1 | *−6.5* | *−1.9* | *3.1* | 0.7 | −0.9 | −0.6 | 0.1 | −0.9 |
| CBCT 2 | *−1.2* | −0.9 | −0.9 | 0.3 | 0.1 | −0.2 | −0.7 | −0.2 | 0.8 | 0.5 | −0.2 | 0.1 | 0.4 | −0.4 |
| CBCT 3 | *−1.2* | −0.9 | −0.9 | −0.3 | −0.4 | −0.8 | *−3.0* | −1.0 | *1.2* | 0.2 | −0.6 | −0.4 | 0.0 | −0.8 |
| CBCT 4 | *−5.9* | *−1.2* | −0.6 | *−1.8* | −0.9 | −0.7 | 0.3 | −1.0 | 0.1 | −0.2 | 0.4 | −0.6 | *−1.4* | *−2.3* |
| CBCT 5 | *−1.9* | −0.8 | −0.7 | 0.2 | 0.0 | −0.3 | *−2.7* | −0.5 | −0.6 | 0.6 | −0.4 | −0.2 | 0.0 | −1.0 |
| CBCT 6 | −0.9 | −0.6 | −0.7 | 0.8 | 0.4 | 0.0 | *−2.7* | 0.2 | −0.4 | 0.8 | −0.2 | 0.2 | 0.3 | −0.5 |
| **Median** | ***−1.2*** | **−0.8** | **−0.8** | **0.2** | **0.0** | **−0.2** | ***−2.7*** | **−0.7** | **0.5** | **0.6** | **−0.3** | **−0.3** | **0.1** | **−0.8** |

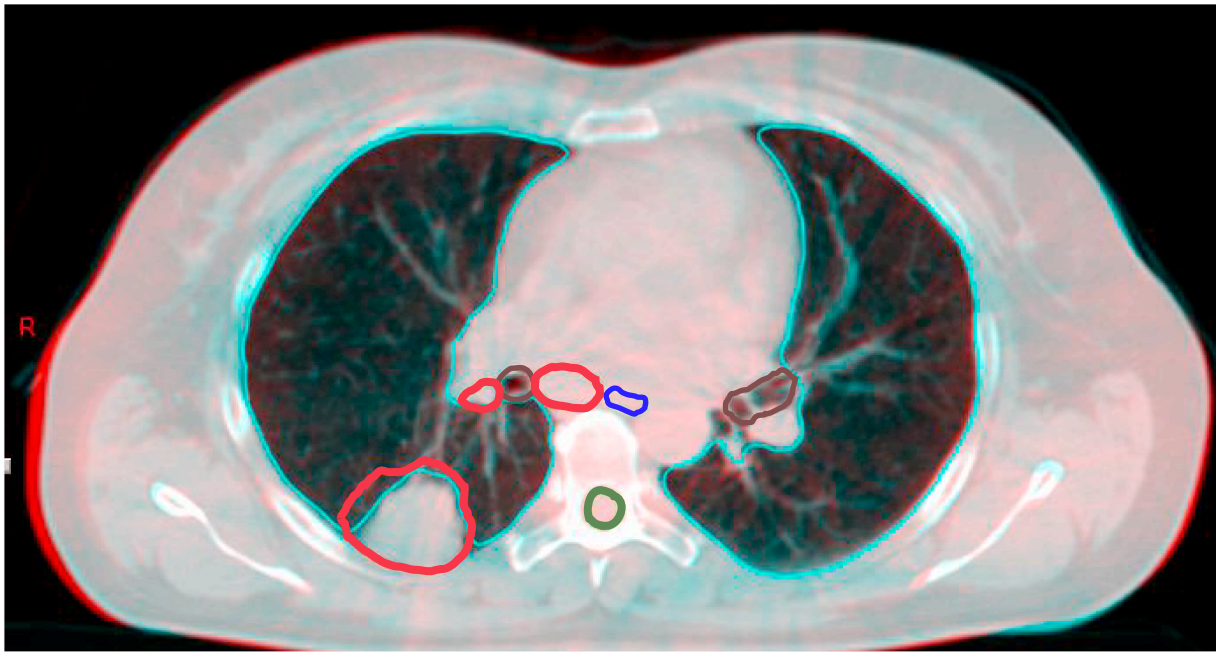


**Fig. 1.** Axial CBCT slice (red) overlaid on the corresponding CT slice (blue) showing a patient included in the study. Both images were acquired at fraction 10. Greyscale colors indicate perfect overlap. Structures shown are delineated on the CT image. Red - target volumes, brown – bronchi, dark green – spinal cord, dark blue – esophagus, light blue – lungs. (For interpretation of the references to colour in this figure legend, the reader is referred to the web version of this article.)

see Fig. 1. The selection was based on a qualitative comparison of patient anatomy on all slices of the surveillance CTs and the CBCTs acquired at the same day for all patients.

Given the very small difference between using a calibration curve determined solely for the CBCT in question and using the mean calibration curve, only the latter was used for dose calculation on patient images. CT and CBCT slices corresponding to the same location in a patient and including 50% and 95% isodoses are shown in Fig. 2. The differences between DVH parameters calculated on the s-CTs and corresponding CBCTs can be seen in Fig. 3. Median CT to CBCT differences for all DVH parameters calculated in all patients were within ± 2%, 93% of all points were within ± 3% and 98% within ± 4%. Some larger outliers were observed; one for the $D_{98}$ to the CTV-T at −4.6%, two for dose to the heart at +9.3% and −5.6%, one for the lung dose at −5.0% and one for the $D_{1cc}$ to the bronchi at −5.2%. The differences of −5.2% in $D_{1cc}$ to the bronchi and +9.3% in $D_{V25Gy}$ to the heart were found to be due to a rotation around the cranio-caudal axis of the CBCT with respect to the s-CT.

The CTV-T $D_{98}$ was underestimated on CBCT for 63% of the patients (median difference −1.9%) independently of tumor size. Underdosage was primarily seen in low density lung tissue as illustrated in Fig. 4. No clear trend for over- or underestimation can be seen for the mean dose. $D_{98}$, mean dose, and $D_{1cc}$ to the mediastinal structures (CTV-N, esophagus, and bronchi) tend to be overestimated on CBCT (median difference +0.6%, +0.8%, +0.6%, +0.8%, respectively).

## 4. Discussion

In this study we have evaluated the use of a stoichiometric HU-to-electron density calibration for direct dose calculation on CBCT images.

The deviation between CBCT and CT doses for the Alderson anthropomorphic phantom is larger than seen for an anthropomorphic head and neck phantom [18] calibrated using the same method. The larger deviation seen in the thorax phantom can be explained by different photon scatter conditions and scan mode, as well as the fact that six CBCT imaging devices were compared in the present study while only one was used by Elstrøm et al [18].

Previously, direct CBCT dose calculations in phantoms using non-stoichiometric calibration methods have been published, with reported CBCT/CT dose differences of approximately 1% [9,17,21]. However, none of these studies considered dose calculation in thorax phantoms. The pronounced photon scatter seen in thorax geometries makes dose calculations more difficult than in e.g. head-and-neck geometries. A stoichiometric calibration of the CBCT scanners has been reported to be more accurate [18,20,22] and was thus used in the present study.

Dose calculation performed on CBCT images of patients showed

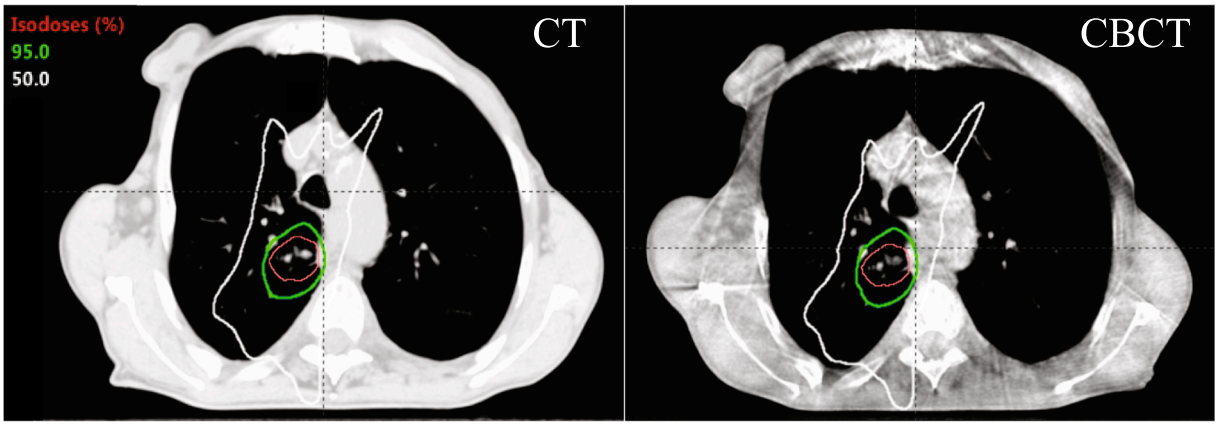


**Fig. 2.** Axial CT/CBCT slices of a lung cancer patient treated with IMRT. The contours show 95% (green) and 50% (white) isodose levels. The thinner pink contour in the center of the 95% isodose shows the CTV-T. (For interpretation of the references to colour in this figure legend, the reader is referred to the web version of this article.)

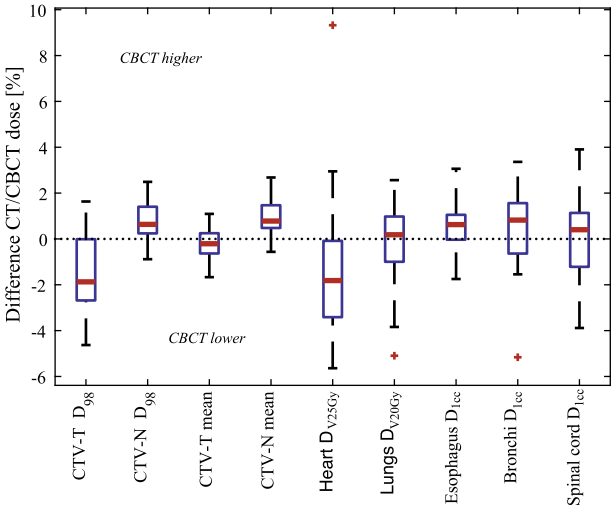


**Fig. 3.** Difference in DVH parameters calculated on CT and CBCT images taken the same day. Each box consists of a maximum of 24 data points, two for each of the 12 patients (fewer if not all patients had the structure in question delineated, e.g. lymph nodes). Red lines denote the median value, blue boxes the 25th to 75th percentiles, whiskers the median ± 2.7σ, and red crosses outliers outside this interval. (For interpretation of the references to colour in this figure legend, the reader is referred to the web version of this article.)

good agreement with the dose calculated on CT images. Compared to previously published methods for CBCT-based dose calculation in lung cancer patients [7,9–13,15], our results show the same level of accuracy (median error below 2% with few outliers). Some studies using HU to electron density calibrations based on patient data achieved higher accuracies at the cost of a larger workload required to perform the calibration [10,12–13].

Under-estimation of the $D_{98}$ to the CTV-T was observed for 63% of the patients, the extent being dependent on tumor location. The largest deviation was seen for tumors situated at the interface of mediastinum and lung tissue. However, for all images, the deviation was below 5%. It is noteworthy that doses to lymph nodes and some mediastinal OARs are over-estimated, in contrast to primary tumors, where underdosage was seen in the low-density lung tissue.

Our previous attempts at direct CBCT dose calculation using our clinical CT HU-to-electron density calibration curve have resulted in over-estimation of doses especially in high-dose areas. Such apparent "hot-spots" might lead to unnecessary replanning of patients. We compared dose calculations using the CT calibration with calculations using the presented CBCT calibration for three patients from this study and found the same: calculated near-maximum doses in the target volumes were between 1% and 1.5% higher when using the CT calibration curve. While this difference seems small, it is an error that is easily improved by performing a careful CBCT calibration.

It should be noted that the Elekta XVI CBCT system used in many of the cited studies [10–15] differs in several key aspects from the Varian Clinac OBI system used in this study and Refs. [9,13,18]; the most notable being scatter correction strategy, HU calibration and field of view [13]. The XVI system has previously shown large HU deviations compared to CT, making HU correction strategies necessary [23]. In fact, many studies using XVI systems performed additional HU correction prior to dose calculation [11–13,15].

The effect of using the presented method together with an experimental CBCT reconstruction algorithm including additional scatter corrections was investigated in an anthropomorphic head and neck phantom by Elstrøm et al [18]. They used the same CBCT imaging systems as described in this study and found no significant difference between standard and scatter-corrected reconstruction. The amount of photon scatter in thorax CBCTs is greater than in head and neck CBCTs, however, so introducing additional scatter corrections may further improve the accuracy of the presented method in thorax geometries.

The workload required to implement the presented method in clinical practice is less than for all the above-mentioned approaches, however, as the calibration procedure is simple and it does not require additional modification of the CBCT images. Furthermore, dose calculations performed using the mean calibration curve on images from six different CBCT scanners gave comparable results. This makes it possible to use a single calibration curve to perform dose calculations on images from all CBCT scanners in use in a department, which facilitates clinical implementation of the method. This is at least true for CBCT scanners of the same model.

While the s-CT and corresponding CBCT were taken on the same day to minimize anatomical deviations, it should be noted that some differences between the images are inherent in the mode of acquisition. The s-CTs are 4DCT scans with structure delineations and dose calculation done on the mid-ventilation phase, while the CBCTs are 3D scans taken in free breathing. The CBCTs thus include motion artefacts to a much greater extent than the s-CTs do. This may lead to a "smearing-out" of moving structures, among these the tumor, in the CBCTs. A dose re-calculation on a motion averaged s-CT image of the patient shown in Fig. 4 showed $< 0.2\%$ difference in tumor $D_2$ and $< 0.1\%$ difference in tumor $D_{98}$ when compared to the original calculation on the mid-ventilation phase. It may thus be assumed that motion-averaging has only a minor effect on the calculated dose. In fact, a very good agreement was found for the delineated tumor and OARs between CT and CBCT.

The use of automated dose calculation on CBCT as a trigger for ART

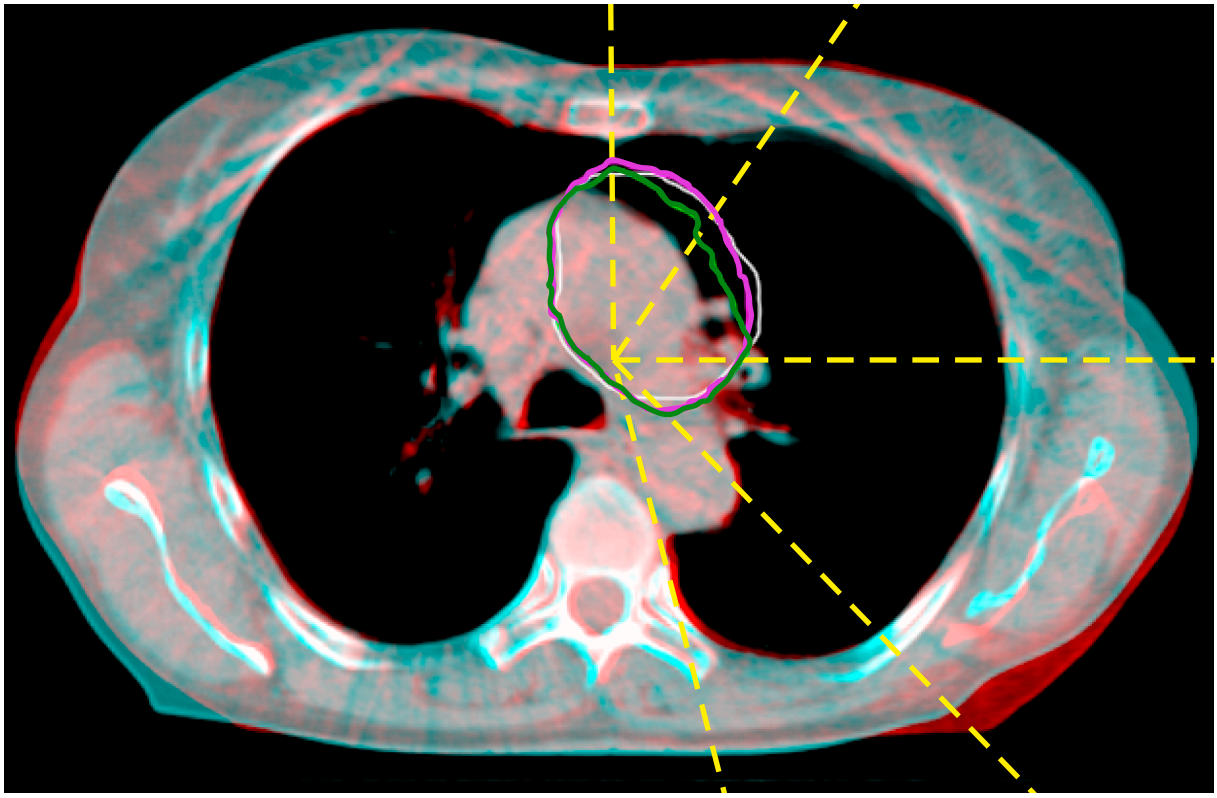

**Fig. 4.** Overlay of s-CT (blue) and CBCT (red) of patient 7 at fraction10. Contours shown are the PTV-T as delineated on the s-CT (white), the 95% isodose curve calculated on the s-CT (pink) and the 95% isodose curve calculated on the CBCT (green). Dashed lines indicate the treatment fields' central axes. (For interpretation of the references to colour in this figure legend, the reader is referred to the web version of this article.)

requires validation of accurate dose calculation and structure propagation from CT to CBCT. The present study shows median differences in dose calculation within ± 2% and combined with a validated contour propagation the method may be used as a tool for a fast off-line dose calculation for all CBCT images acquired on a daily basis. The method can be used to raise a flag for those scans where the dose deviation has been found to be outside the pre-set limit.

Our results show that a careful, phantom-based HU-to-electron density calibration of the CBCT scanners enables daily CBCT-based dose calculation with median error < 2% and 98% of the evaluated points are within ± 4%. The method is easily implemented in a clinical workflow.

## Conflict of interest statement

All authors declare no conflictof interest.

## Acknowledgements

This research was supported by a grant from the Danish Cancer Society.

## Appendix A. Supplementary data

Supplementary data to this article can be found online at https://doi.org/10.1016/j.phro.2018.09.001.

## References

[1] Møller DS, Khalil AA, Knap MM, Hoffmann L. Adaptive radiotherapy of lung cancer patients with pleural effusion or atelectasis. Radiother Oncol 2014;110:517–22.
[2] Kwint M, Conijn S, Schaake E, Knegjens J, Rossi M, Remeljer P, et al. Intra thoracic anatomical changes in lung cancer patients during the course of radiotherapy. Radiother Oncol 2014;113:392–7.
[3] Britton KR, Starkschall G, Liu H, Chang JY, Bilton S, Ezhil M, et al. Consequences of anatomic changes and respiratory motion on radiation dose distributions in conformal radiotherapy for locally advanced non-small-cell lung cancer. Int J Radiat Oncol Biol Phys 2009;73:94–102.
[4] Schmidt ML, Hoffmann L, Kandi M, Møller DS, Poulsen PR. Dosimetric impact of respiratory motion, interfraction baseline shifts, and anatomical changes in radiotherapy of non-small cell lung cancer. Acta Oncol 2013;52:1490–6.
[5] Møller DS, Holt MI, Alber M, Tvilum M, Khalil AA, Knap MM, et al. Adaptive radiotherapy for advanced lung cancer ensures target coverage and decreases lung dose. Radiother Oncol 2016;121:32–8.
[6] Hoffmann L, Knap MM, Khalil AA, Lutz CM, Møller DS. The NARLAL2 dose escalation trial: dosimetric implications of inter-fractional changes in organs at risk. Acta Oncol 2017;23:1–7.
[7] Veiga C, Janssens G, Teng CL, Baudier T, Hotoiu L, McClelland JR, et al. First clinical investigation of cone beam computed tomography and deformable registration for adaptive proton therapy for lung cancer. Int J Rad Oncol Biol Phys 2016;91:549–59.
[8] Elstrøm UV, Wysocka BA, Muren LP, Petersen JBB, Grau C. Daily kV cone-beam CT and deformable image registration as a method for studying dosimetric consequences of anatomic changes in adaptive IMRT of head and neck cancer. Acta Oncol 2010;49:1101–8.
[9] Yang Y, Schreibmann E, Li T, Wang C, Xing L. Evaluation of on-board kV cone beam CT (CBCT)-based dose calculation. Phys Med Biol 2007;52:685–705.
[10] Fotina I, Hopfgartner J, Stock M, Steininger T, Lütgendorf-Caucig C, Gerog D. Feasibility of CBCT-based dose calculation: comparative analysis of HU adjustment techniques. Radiother Oncol 2012;104:249–56.
[11] Dunlop A, McQuaid D, Nill S, Murray J, Poludniowski G, Hansen VN, et al. Comparison of CT number calibration techniques for CBCT-based dose calculation. Strahlenther Onkol 2015;191:970–8.
[12] Richter A, Hu Q, Steglich D, Baier K, Wilbert J, Guckenberger M, et al. Investigation of the usability of cone-beam CT data sets for dose calculation. Radiat Oncol 2008;3:42–55.
[13] de Smet M, Schuring D, Nijsten S, Verhaegen F. Accuracy of dose calculations on kV cone beam CT images of lung cancer patients. Med Phys 2016;43:5934–41.
[14] Thing RS, Bernchou U, Mainegra-Hing E, Hansen O, Brink C. Hounsfield unit recovery in clinical cone beam CT images of the thorax acquired for image guided radiation therapy. Phys Med Biol 2016;61:5781–802.
[15] Thing RS, Bernchou U, Hansen O, Brink C. Accuracy of dose calculation based on artefact corrected Cone Beam CT images of lung cancer patients. Phys Imaging Radiat Oncol 2017;1:6–11.
[16] Poludniowski GG, Evans PM, Webb S. Cone beam computed tomography number errors and consequences for radiotherapy planning: an investigation of correction methods. Radiat Oncol 2012;84:e109–14.

[17] Elstrøm UV, Olsen SK, Wysocka BA, Muren LP, Petersen JBB, Grau C. A direct comparison of cone-beam CT versus CT based radiotherapy planning in head and neck cancer. Radiother Oncol 2012;102:S139.
[18] Elstrøm UV, Olsen SRK, Muren LP, Petersen JBB, Grau C. The impact of CBCT reconstructionand calibration for radiotherapy planning in the head and neck region – a phantom study. Acta Oncol 2014;53:1114–24.
[19] Schneider U, Pedroni E, Lomax A. The calibration of CT Hounsfield units for radiotherapy treatment planning. Phys Med Biol 1996;41:111–24.
[20] Schneider W, Bortfeld T, Schlegel W. Correlation between CT numbers and tissue parameters needed for Monte Carlo simulations of clinical dose distributions. Phys Med Biol 2000;45:459–78.
[21] Hatton J, McCurdy B. Greer PB Cone beam computerized tomography: the effect of calibration of the Hounsfield unit number to electron density on dose calculation accuracy for adaptive radiation therapy. Phys Med Biol 2009;54:N329–46.
[22] Guan H, Yin F-F, Kim JH. Accuracy of inhomogeneity correction in photon radiotherapy from CT scans with different settings. Phys Med Biol 2002;47:N223–31.
[23] van Zijtveld M, Dirkx M, Heijmen B. Correction of conebeam CT values using a planning CT for derivation of the “dose of the day”. Radiother Oncol 2007;85:195–200.